Crystal structure of rilpivirine hydrochloride, $N_6H_{19}C_{22}Cl$

Petr Buikin,[1,2] Alexander Korlyukov,[1] Elizaveta Kulikova,[3] Roman Novikov,[4] and Anna Vologzhanina [1,a)]
[1]A. N. Nesmeyanov Institute of Organoelement Compounds RAS, Vavilova Str. 28, Moscow 119334, Russia
[2]Institute of General and Inorganic Chemistry RAS, Leninsky Prosp. 31, Moscow 119991, Russia
[3]Kurchatov Institute, National Research Center, Pl. Akad. Kurchatova 1, Moscow123182, Russia
[4]N. D. Zelinsky Institute of Organic Chemistry, RAS, Leninsky Prosp. 47, Moscow 119991, Russia

(Received 1 November 2023; accepted 6 April 2024)

A monoclinic *C* form of rilpivirine hydrochloride, $(N_6H_{19}C_{22})Cl$, has been obtained and characterized using solid-state ^{15}N, ^{13}C, and ^{35}Cl NMR spectroscopy and multitemperature synchrotron X-ray powder diffraction. The title compound crystallizes in the monoclinic system (space group *C*2/*c*, #15) at both room (295.0(2) K) and low (100.0(2) K) temperatures. At room temperature, the following parameters are $a = 19.43051(3)$, $b = 13.09431(14)$, $c = 17.10254(18)$ Å, $\beta = 109.3937(7)$, $V = 4104.48(9)$ Å^3, and $Z = 8$. The folded molecular conformation of the cation is similar with that of free base rilpivirine with the exception of cyanovinyl group disposition. The anion links cations to infinite chains parallel to the crystallographic *c* axis using N–H⋯Cl bonds where both amino groups and the protonated pyrimidine ring take part in the H-bonding. The powder patterns have been submitted to the ICDD for inclusion in the Powder Diffraction File™ (PDF®).
© *The Author(s), 2024. Published by Cambridge University Press on behalf of International Centre for Diffraction Data.*
[doi:10.1017/S0885715624000228]

Key words: multitemperature study, powder diffraction, Rietveld refinement, rilpivirine

I. INTRODUCTION

The number of drugs based on active pharmaceutical ingredients (API) in the form of salts has increased in the past decades (Wermuth and Stahl, 2001) due to the potential of multi-component solids to tune stability (Dhondale et al., 2023), solubility, or tabletability (Paulekuhn et al., 2007; Braga et al., 2011) of medications. However, the development of new drugs based on multicomponent solids can be hindered by the lack of high-quality reference powder patterns and/or crystal structures required for phase identification and quantitative analysis by the pharmaceutical industry (Hilfiker et al., 2006). Thus, recent progress in algorithms for structure solutions from powder XRD data and an increase in computational resources resulted in increases of crystal structures of multicomponent API solids obtained from powder X-ray diffraction (XRD). The following examples are besifloxacin hydrochloride (Kaduk et al., 2023a), butenafine hydrochloride (Kaduk et al., 2023b), carbamazepine cocrystals (Guerain et al., 2020; Surov et al., 2023), zonisamide/ϵ-caprolactam cocrystal (Barbas et al., 2022).

Rilpivirine (DrugBank No. DB08864) is a non-nucleoside reverse transcriptase inhibitor used for the treatment of HIV-1 in treatment-naive adults (Putcharoen et al., 2013). The crystal structure of free base rilpivirine has been solved by means of powder X-ray diffraction by Kaduk et al. (2015). However, the commercially available medication Edurant contains rilpivirine in the form of hydrochloride (Scheme 1). Patents WO2012125993A1 (Rendell et al., 2012), WO2013153161A2 (Hotter et al., 2013), and EP2628732A1 (Sandoz, 2013) and paper by Kommavarapu et al. (2015) contain information about polymorphs and solvates of rilpivirine hydrochloride; however, data about crystal structures of any rilpivirine salts are still missing. Within our research devoted to XRD characterization of solid forms of known APIs (Goloveshkin et al., 2021; Korlyukov et al., 2022, 2023; Buikin et al., 2023), the crystal structure of the title compound has been obtained by means of synchrotron powder X-ray diffraction. The solid was also characterized by means of solid-state ^{13}C, ^{15}N, and ^{35}Cl NMR spectroscopy.

II. EXPERIMENTAL

Rilpivirine substance was purchased from Clearsynth (CAS No. 700361-47-3) and used without any purification. The infra-red (IR) spectrum of the substance was recorded on an IR spectrometer with a Fourier transformer Shimadzu IRTracer100 (Kyoto, Japan) in the range of 4000–600 cm^{-1} at a resolution of 1 cm^{-1} (Nujol mull, KBr pellets) and coincided with that published before (Kommavarapu et al., 2015). ^{15}N and ^{13}C NMR solid-state NMR experiments were recorded on a Bruker AVANCE III WB 400 MHz spectrometer equipped with a 4.0 mm magic angle sample spinning (MAS) BB/HF probe (15 kHz) and a 2.5 mm MAS BB/H probe (35 kHz) (^1H – 400.1 MHz, ^{13}C – 100.6 MHz, ^{15}N – 40.6 MHz, and ^{35}Cl – 39.2 MHz). Samples were spun at 9.5–14 kHz (4.0 mm probe) at the magic angle (MAS) using ZrO_2 rotors. ^{13}C cross-polarization / magnetic angle spinning (CP/MAS) spectra were recorded with a recycle delay of 8 s and contact times of 3 ms at 13 kHz. ^{15}N-CP/MAS spectra were recorded with a recycle delay of 14–18 s and contact

a)Author to whom correspondence should be addressed. Electronic mail: vologzhanina@mail.ru

https://doi.org/10.1017/S0885715624000228 Published online by Cambridge University Press

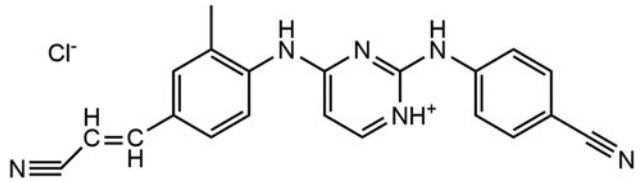

Scheme 1. The molecular structure of rilpivirine hydrochloride.

times of 6–15 ms at 9.5 kHz. ^{1}H MAS spectra were recorded using single-pulse sequences at 14 kHz (4.0 mm probe) and 34 kHz (2.5 mm probe) with a recycle delay of 15 s. ^{35}Cl MAS spectra were recorded using Hahn-Echo pulse sequences at 14 kHz (4.0 mm probe) in a rotor-synchronized mode using 63.2 µs echo-time (1 rotor cycle) with a recycle delay of 0.5 s. 2D ^{13}C–^{1}H CP-FSLG-HETCOR spectra were recorded at 13 kHz MAS (4.0 mm probe) in a rotor-synchronized mode using 300–2100 µs contact time under CP conditions to detect direct/long-range C–H correlations. All the ^{13}C, ^{15}N, and 2D HETCOR spectra were recorded under high-power proton decoupling conditions using "spinal64". All chemical shifts for ^{1}H and ^{13}C are relative to the external adamantane sample; ^{15}N chemical shifts were calculated to this scale and were checked using the ^{15}N-labeled-glycine sample; ^{35}Cl chemical shifts are relative to the external NaCl sample.

Elemental analysis was calculated for $C_{22}H_{19}ClN_6$ (%): C 65.5; H 4.7; Cl 8.9; N 20.9. Found (%): C 65.46(12); H 4.86 (4); Cl 9.04(8); N 20.64(10).

A. Powder X-ray diffraction

The synchrotron PXRD data were recorded at the X-ray structural analysis beamline (Belok/XSA) of the Kurchatov Synchrotron Radiation Source (Svetogorov et al., 2020). Monochromatic radiation was used to measure the pattern and then θ angles were recalculated to a wavelength of 0.7500 Å. The sample was placed in a cryoloop of 200 μm in size and rotated around the horizontal axis during the measurement, which made it possible to average the diffraction patterns according to the orientations of the sample. The diffraction patterns were collected by the 2D Rayonix SX165 detector, which was located at a distance of 150 and 250 mm with 29.8 and 18° tilt angles, respectively, Debye–Scherrer (transmission) geometry was used with a 400 μm beam size. The 2θ range was 0.99–59.8° with a step size of 0.00994°. The exposure time was 10 min. The two-dimensional diffraction patterns obtained on the detector were further integrated to the standard form of the dependence of the intensity on the scattering angle $I(2\theta)$ using the Dionis software (Svetogorov, 2018). To calibrate the sample–detector distance, the polycrystalline LaB_6 (NIST SRM 660a) was used as a standard with the known position of the diffraction peaks. The diffraction peaks were approximated by fundamental parameters with Gaussian $1/\cos(\theta)$ convolution.

The indexing of the powder pattern and the subsequent structure solution were performed with the Topas 5.0 software (Coelho, 2003; Bruker TOPAS 5 User Manual, 2014). All patterns were indexed in the *C*-centered monoclinic unit cell. The systematic absences suggested the space group *C*2/*c*, which was confirmed by the successful solution and refinement of the structure. A molecular model of rilpivirine was taken from a publication by Kaduk et al. (2015) and converted into a Fenske–Hall Z-matrix file using OpenBabel (O'Boyle et al., 2011). A simulated annealing algorithm of the Topas 5.0 software was applied to find the position of non-hydrogen atoms of rilpivirine and an independent chlorine atom in an asymmetric unit. The solution result was used as a starting geometry for the periodic density functional theory (DFT) calculations at PBE (Perdew–Baron–Erzenhopf) exchange–correlation functional level with the fixed unit cell using VASP 5.4.1 (Kresse and Hafner, 1993, 1994; Kresse and Furthmüller, 1996a, 1996b). Atomic cores were described using projected augmented wave (PAW) potentials (Blöchl, 1994; Kresse and Joubert, 1999). Valence electrons were described in terms of a plane-wave basis set.

Optimization result with the fixed unit cell was used as the starting geometry, and the sources of bond and angle restraints in the Rietveld refinement (Rietveld, 1967) were used for synchrotron powder XRD data. Atomic coordinates were taken from the PBE-PAW optimized model and refined with the Topas 5.0 software. Anisotropic displacement parameters were refined equally for three types of carbon atoms, all chlorine, and all nitrogen. The positions of the hydrogen atoms were calculated geometrically and refined in the riding model with $U_{iso}(H) = 1.5U_{iso}(C)$ for methyl groups and $1.2U_{iso}(X)$ for other atoms. The final *R*-values are listed in Table I along with the corresponding values of Rietveld refinement results. Average/maximal atomic deviations of models I, II, III, and IV from the optimized model were equal to 0.06/0.11, 0.08/0.15, 0.06/0.12, and 0.08/0.15 Å. The comparison of the optimized model and model I (150 mm, 100 K) indicates that the majority of deviations corresponds to positions of methyl groups (Supplementary Figure S1). The Rietveld plot recorded at room temperature (RT) at 250 mm distance is given in Figure 1, and the other plots are given in Supplementary Material (Supplementary Figure S2).

B. Computational methods

The plane-wave calculations were carried out in the VASP 5.4.1 program package (Kresse and Hafner, 1993, 1994; Kresse and Furthmüller, 1996a, 1996b). The PBE method (Perdew et al., 1999) and PAW (Kresse and Joubert, 1999; Kresse and Hafner, 2000) were used. Valence electrons (2s and 2p for O, N, and C atoms; 1s for H) were described in terms of a plane-wave basis set. The kinetic energy cutoff for the wave functions was set to 800 eV. Automatic *k*-point sampling was used. The total energy and force convergence thresholds were set to 10^{-6} and 10^{-4} eV, respectively. The crystal structures from the powder X-ray diffraction experiment were used as the starting geometry for the calculations. The geometry optimizations were carried out with the lattice parameters fixed at their crystallographic values. The output files with the relaxed geometries were converted to a res-file using VESTA (Momma and Izumi, 2011).

III. RESULTS AND DISCUSSION

A. Details of structure refinement

Previously reported polymorphs of rilpivirine hydrochloride were characterized using laboratory diffractometers with CuK_α radiation at RT. None of the reported patterns was

https://doi.org/10.1017/S0885715624000228 Published online by Cambridge University Press

TABLE I. Crystal data and structure refinement for rilpivirine hydrochloride.

Identification code	150 mm/100 K (**I**)	150 mm/298 K (**II**)	250 mm/100 K (**III**)	250 mm/298 K (**IV**)
Empirical formula	$N_6H_{19}C_{22}Cl$	$N_6H_{19}C_{22}Cl$	$N_6H_{19}C_{22}Cl$	$N_6H_{19}C_{22}Cl$
Formula weight	402.87	402.87	402.87	402.87
Temperature (K)	100	298	100	298
Crystal system	Monoclinic	Monoclinic	Monoclinic	Monoclinic
Space group	*C*2/*c*	*C*2/*c*	*C*2/*c*	*C*2/*c*
a (Å)	19.4327(5)	19.4348(4)	19.4360(3)	19.4305(3)
b (Å)	12.9755(3)	13.1861(2)	12.97727(15)	13.09431(14)
c (Å)	17.0195(3)	17.1399(3)	17.0200(2)	17.10252(18)
α (°)	90	90	90	90
β (°)	109.4804(15)	109.3746(12)	109.4837(9)	109.3937(7)
γ (°)	90	90	90	90
Volume (Å^3)	4045.78(17)	4143.70(13)	4047.08(10)	4104.48(9)
Z	8	8	8	8
ρ_{calc} (g · cm^{-3})	1.323	1.292	1.322	1.304
F(000)	1680	1680	1680	1680
Radiation	Synchrotron ($\lambda = 0.75$)	Synchrotron ($\lambda = 0.75$)	Synchrotron ($\lambda = 0.75$)	Synchrotron ($\lambda = 0.75$)
2Θ range for data collection (°)	0.99–59.8	0.99–59.8	0.33–38.13	0.33–38.1
Reflections collected	2624	2624	956	956
Data/restraints/parameters	5882/73/251	5882/73/251	6201/73/248	6101/73/246
Goodness-of-fit on F^2	0.153	0.182	0.224	0.253
R-Bragg (%)	0.438	0.414	0.817	1.007
Final *R* indexes (%)	$R_{exp} = 4.886$, $R_{wp} = 0.759$, $R_p = 0.565$	$R_{exp} = 4.209$, $R_{wp} = 0.766$, $R_p = 0.562$	$R_{exp} = 6.372$, $R_{wp} = 1.430$, $R_p = 1.019$	$R_{exp} = 6.847$, $R_{wp} = 1.735$, $R_p = 1.230$

indexed (Rendell et al., 2012; Hotter et al., 2013; Sandoz, 2013; Kommavarapu et al., 2015). For our structure obtained from RT data (sample **IV**), theoretically calculated pattern for CuK_α radiation comprises characteristic peaks at $2\theta = 9.1$, 9.6, 11.0, 12.0, 13.7, 14.7, and 15.1° (Supplementary Figure S3), which correspond to the anhydrous rilpivirine hydrochloride described by Kommavarapu et al. (2015). IR spectrum for this sample contains weak bands, which can be associated with secondary amine stretching vibrations observed at 3477 and 3404 cm^{-1}. Besides, two strong bands at 1599 and 1516 cm^{-1} appear in the spectrum, which correspond to NH^+ bending vibrations.

Based on the powder XRD pattern described at US2010189796 patent (Stokbroekx, 2010), Kaduk et al. (2015) reported the crystal structure of Form II of free base rilpivirine, which is characterized by characteristic bands in IR spectra at 3316 ($\nu(R_2NH)$ group), 2223 (ν(C≡N)), 2215 (ν(C≡N)), 1483 (aromatic ν(C–C)), and 1325 (δ(=CH)) cm^{-1}. For our salt, bathochromic shift of the $\nu(R_2NH)$ band denotes weakening of the N–H···N hydrogen bond in rilpivirine as compared with the N–H···Cl bonds in rilpivirine hydrochloride.

As it follows from Table I, at a given detector distance, the quality of refinement and convergence factors are almost independent on the temperature of the experiment. Thus, ambient condition powder data are more valuable for phase identification, while low-temperature data are more helpful for structure solution and refinement. In the latter cases, thermal motion is

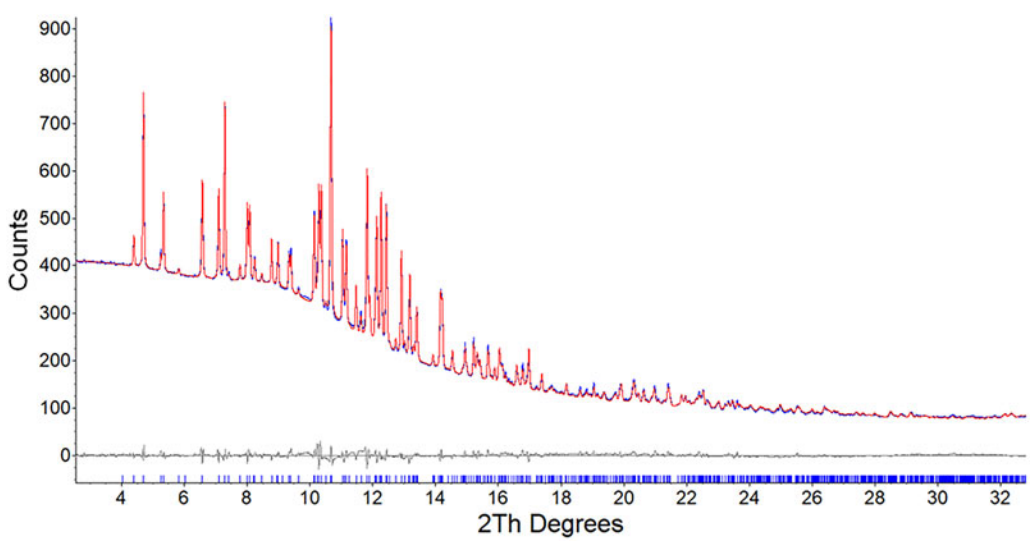

Figure 1. XRD pattern **IV**. Red and blue lines correspond to the calculated profile and experimental patterns, respectively. The bottom trace shows the difference curve.

https://doi.org/10.1017/S0885715624000228 Published online by Cambridge University Press

TABLE II. Isotropic thermal parameters of atoms ($Å^2$).

Atom	150 mm/ 100 K (**I**)	150 mm/ 298 K (**II**)	250 mm/100 K (**III**)	250 mm/298 K (**IV**)
Cl	0.047(2)	0.054(1)	0.040(2)	0.028(1)
N	0.040(2)	0.060(1)	0.032(3)	0.036(1)
C	0.035(4)	0.045(2)	0.034(4)	0.035(2)
C_{Ph}	0.033(3)	0.057(2)	0.026(4)	0.029(1)
C_{Cyano}	0.040(2)	0.047(2)	0.031(4)	0.046(2)

lower that simplifies the determination of molecular conformation and packing. Isotropic thermal parameters of atoms are listed in Table II. Indeed, the temperature increase is accompanied by an increase in U_{iso} values from 0.001 to 0.024 $Å^2$. The distance between the sample and the detector in our case strongly affects convergence factors and standard deviations. For the 250 mm distance, deviations for cell parameters are lower due to more sharp peaks at low angles (Supplementary Figure S2). At the same time, all convergence factors (R_{int}, R_{wp}, R_p, R-Bragg) at this distance are higher than those for data obtained at the 150 mm distance. This fact is related to a lower number of observed reflections (2624 vs. 956 reflections for 150 and 250 mm). However, for the 150 mm distance, the pattern becomes nearly linear at $2\theta > 30°$; and difference between peaks becomes negligible. Although this fact allows to decrease all R-factors, it, in fact, does not affect the overall quality of refinement. Finally, more Chebychev coefficients are required for the refinement of background (8th order for **I** vs. 5th order for **III**). Thus, despite higher convergence factors, structure solution and the refinement of small organic molecules from synchrotron radiation obtained at the NIC "Kurchatov Institute" should be carried out using the 250 mm distance between a sample and the detector. Note that, for large-volume unit cell samples, the sample-to-detector distance should likely be decreased.

B. Molecular and crystal structures of rilpivirine hydrochloride

The asymmetric unit of this salt contains one protonated rilpivirine molecule and a chloride anion (Figure 2). The protonated atom of the cation was revealed from DFT calculations, ^{15}N NMR solid-state spectrum, and the most probable H-bonding system as well. In accord with these data, the pyrimidine ring is protonated, so that the H(N) atom is able to take part in N–H···Cl bonding, while the second nitrogen atom of the heterocycle is involved in intramolecular C–H···N bonding. This bonding supports the delocalization of the lone pair of the amine N23 nitrogen. This is indicated by the similarity in C–N23 distances (1.361 and 1.366 Å), and N6–C5–N23–C24 and C5–N23–C24–C25 torsion angles (12.1 and 11.6°). Instead, the lone pair of the N10 amine nitrogen is probably delocalized only with heterocycle. The delocalization manifests itself through asymmetry of bond lengths (1.283 Å for C9–N10 and 1.471 Å for C11–N10) and torsion angles (2.6 and 90.0° for C11–N10–C9–C8 and C9–N10–C11–C12). Overall molecular conformation is folded; it is close to that of free base rilpivirine (Kaduk et al., 2015) (Figure 3), with the exception of positions of substituted phenyl rings and the cyanovinyl group due to rotation along single C–N amine and C–C bonds.

Each molecule takes part in H-bonding with two chloride anions by N–H···Cl interactions. The parameters of these bonds for the theoretical model are listed in Table III. The anions and cations are connected by these bonds into infinite chains parallel to the crystallographic c axis (Figure 4). Besides, the anions are involved in weak C–H···Cl bonding

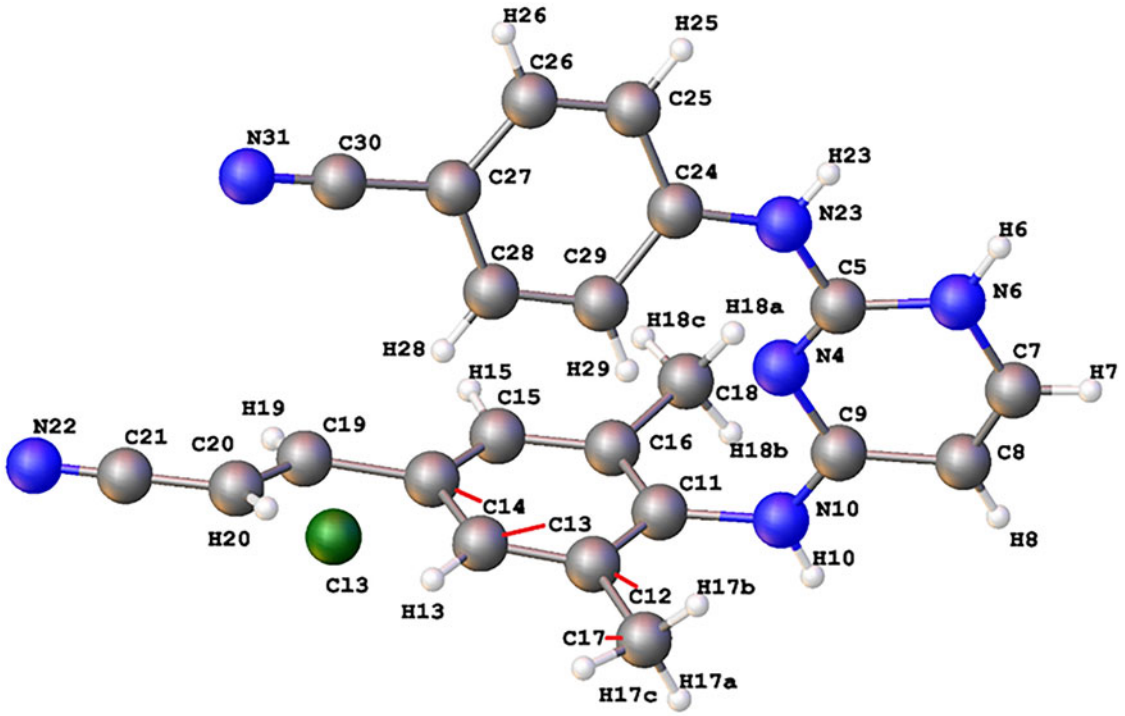

Figure 2. Asymmetric unit of rilpivirine hydrochloride.

https://doi.org/10.1017/S0885715624000228 Published online by Cambridge University Press

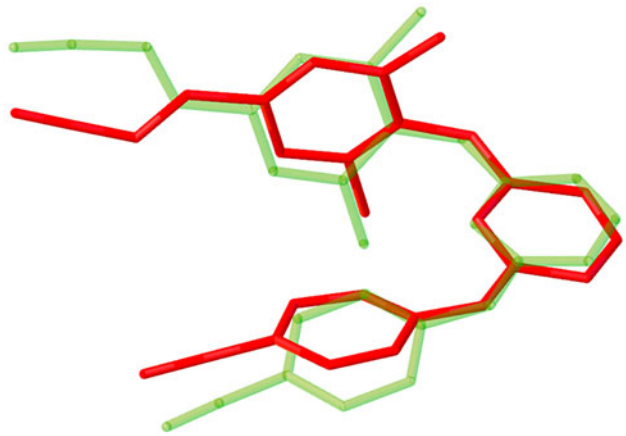

Figure 3. Molecular conformations of rilpivirine in pure solid (green) and rilpivirine hydrochloride (red).

TABLE III. Parameters of H-bonds in the theoretical model of rilpivirine hydrochloride.

D–H···A	D–H (Å)	H···A (Å)	D···A (Å)	<(DHA) (°)
N10–H10···Cl3	1.039	2.127	3.138	163.7
N6–H6···Cl3	1.038	2.237	3.174	149.4
N23–H23···Cl3	1.037	2.224	3.189	154.0

that connects the chains into a 3D framework. These are two C–H···Cl bonds with one molecule, which support the folded conformation of the cation (Figure 2) and a bond with a hydrogen atom of the heterocycle of another molecule.

C. Solid-state ^{15}N and ^{13}C NMR spectroscopy

Full analysis of solid-state NMR ^{13}C and ^{15}N chemical shifts has been undertaken. ^{35}Cl NMR has also been recorded (Supplementary Figure S4), which confirmed the presence of the chloride anion in the solid phase; however, full analysis of chemical shifts has not been carried out yet. Rilpivirine hydrochloride in the solid state is represented by one polymorph with the ordered structure as follows from sharp peaks in ^{13}C and ^{15}N NMR spectra (Figures 5 and 6). 2D solid-state ^{13}C-^{1}H HETCOR NMR experiments with varied contact times were applied to investigate ^{13}C–^{1}H interactions (Figure 7). Solid-state NMR spectra and NMR ^{13}C and ^{15}N spectra in solution were also compared. In general, solid-state spectra correspond well with those in solution, although some chemical signals are significantly shifted. Besides, symmetrical signals corresponding to benzene rings due to their free rotation in solution are affected by the asymmetrical environment in solids; the signals corresponding to ortho- and meta-positions become double. ^{15}N SSNMR spectra are valuable for the analysis of N···H hydrogen bonds in the solid. It is clearly seen that the N6 atom of a pyrimidine ring was protonated: the corresponding signal is upfield shifted compared to the solution more than signals from other atoms. Besides, in solution, evidence of protonation is less pronounced probably due to a dynamic equilibrium.

Besides the analysis of experimental solid-state NMR spectra, the quantum chemical calculations of chemical shifts were carried out. To calculate the values of chemical shifts, we used optimized geometry of the rilpivirin hydrochloride (theoretical model). The ability to calculate chemical shifts is implemented in the VASP 5.4.1 code; however, the usage of PAW potentials to account for core electrons can be considered as a potential source of errors. To bring the calculated values of chemical shifts into the same scale as experimental ones, we used values of isotropic chemical shifts of ^{15}N and ^{13}C calculated for preliminary optimized crystal structures of ammonia and orthorhombic $SiMe_4$. The results of chemical shift calculations are summarized in Supplementary Table S3 and Figure S4. The differences in experimental and calculated values do not exceed 18.0 and 12.1 ppm for ^{15}N and ^{13}C chemical shifts. The most pronounced disagreement between the experiment and quantum chemical calculations is observed in the case of cyano groups and carbon atoms surrounded by acceptor nitrogen atoms (C5 and C9). In general, the presence of a nitrogen atom bonded to C1 leads to an increase in difference between experiment and calculated values of chemical shifts. On the other hand, the chemical shifts for methyl groups are reproduced within 3 ppm. For the most of carbon atoms of phenyl groups, the differences are as low as 10 ppm. The observable disagreement for the most part can be corrected using simple linear regression (Supplementary Figure S5). After the differences between experimental and calculated chemical shifts became satisfactory. As a result, we can conclude that the solid-state NMR study of rilpivirine hydrochloride is in agreement with the structure derived from powder X-ray data.

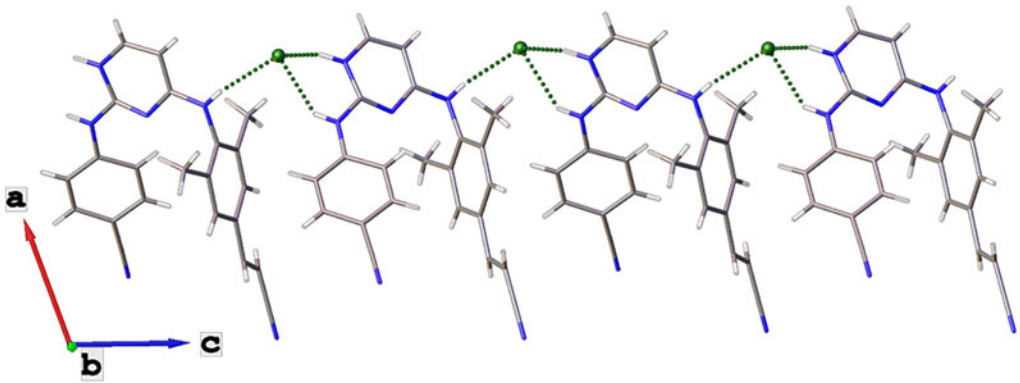

Figure 4. Fragment of N–H···Cl-bonded chains in rilpivirine hydrochloride. H-bonds are depicted with dotted lines.

https://doi.org/10.1017/S0885715624000228 Published online by Cambridge University Press

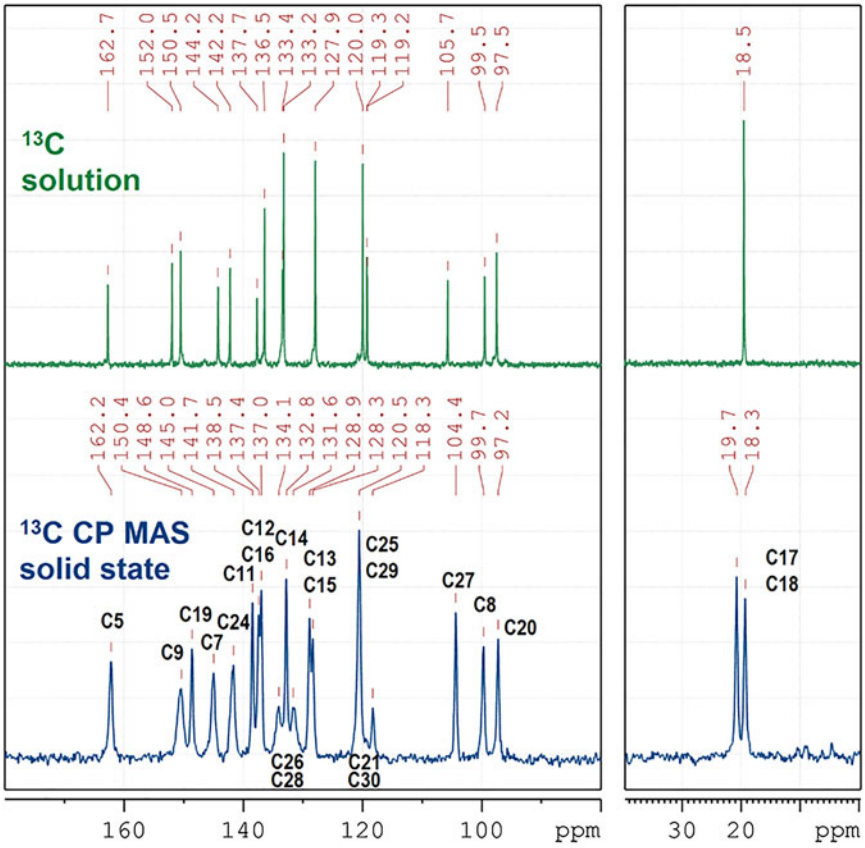

Figure 5. ^{13}C CP MAS (13 kHz) solid-state NMR spectrum of powder Rilpivirin-HCl with full signal assignment, and comparison with ^{13}C spectrum in DMSO solution (top). Atomic numeration is given in Figure 2.

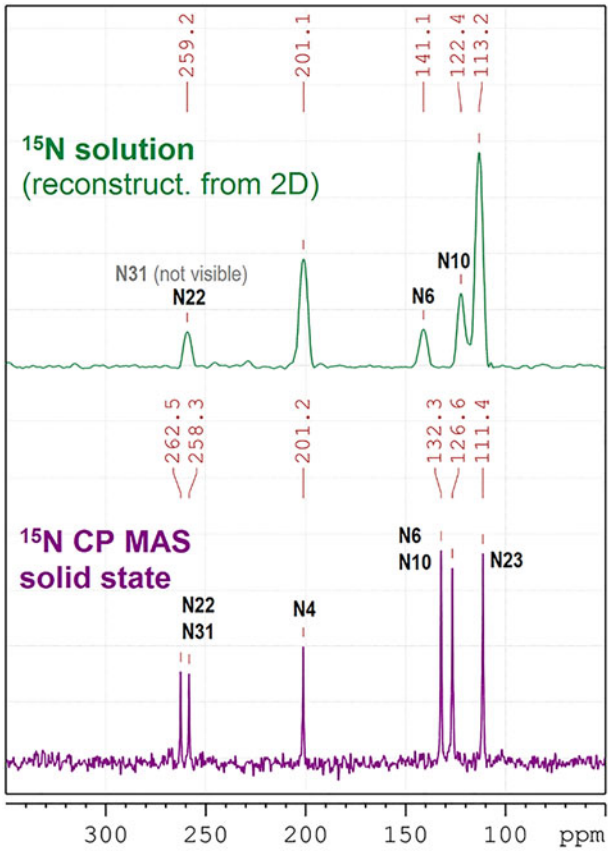

Figure 6. ^{15}N CP MAS (9.5 kHz) solid-state NMR spectrum of powder Rilpivirin-HCl with full signal assignment, and comparison with ^{15}N spectrum in DMSO solution (reconstructed from 2D HSQC and HMBC) (top). Atomic numeration is given in Figure 2.

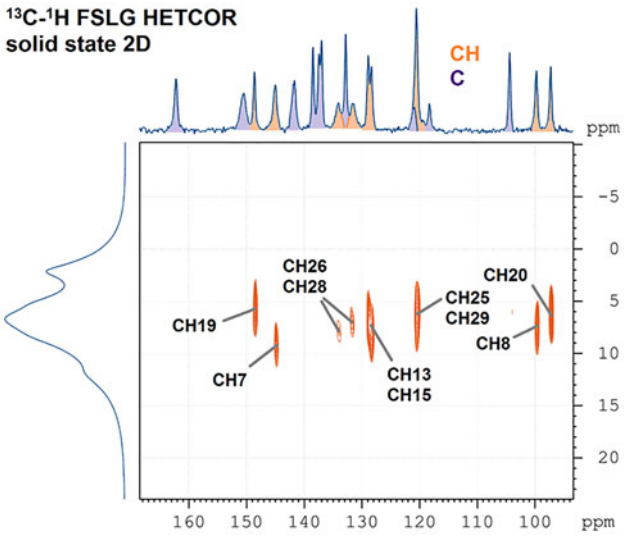

Figure 7. 2D ^{13}C-^{1}H FSLG HETCOR solid-state NMR spectrum (13 kHz MAS) used for signal analysis and assignment. Atomic numeration is given in Figure 2.

IV. CONCLUSION

The molecular and crystal structure of rilpivirine hydrochloride, which is used as an active pharmaceutical ingredient in an anti-HIV medication, has been studied at both RT and low temperature using synchrotron radiation and powder XRD data. No phase transition was observed. The solution is in accord with solid-state ^{15}N and ^{13}C NMR data. The analysis of convergence factors and standard deviations for different sample–detector distances revealed that powder patterns of

https://doi.org/10.1017/S0885715624000228 Published online by Cambridge University Press

small organic molecules from synchrotron radiation obtained at the NIC "Kurchatov Institute" should be obtained using the 250 mm distance between a sample and the detector.

V. DEPOSITED DATA

Four powder patterns of the title compound from synchrotron data obtained at 100 and 298 K at two detector distances (150 and 250 mm) have been submitted to the ICDD for inclusion in the Powder Diffraction File. The CIF files (CCDC 2303885-2303888) can also be obtained at www.ccdc.cam.ac.uk/structures.

Crystallographic Data Files were deposited with ICDD. Files can be requested by contacting the Managing Editor at pdj@icdd.com.

SUPPLEMENTARY MATERIAL

The supplementary material for this article can be found at https://doi.org/10.1017/S0885715624000228.

ACKNOWLEDGEMENTS

This research was funded by the Russian Science Foundation (grant no. 23-73-00027). Solid-state NMR experiments were performed using the solid-state NMR facility at the Department of Structural Studies of N. D. Zelinsky Institute of Organic Chemistry of the RAS, Moscow (R.N.).

CONFLICTS OF INTEREST

The authors declare no conflicts of interest.

REFERENCES

Barbas, R., A. Portell, R. Prohens, and A. Frontera. 2022. "DFT–Assisted Structure Determination from Powder X-ray Diffraction Data of a New Zonisamide/ϵ-Caprolactam Cocrystal." *Crystals* 12 (8): 1020. doi:10.3390/cryst12081020.

Blöchl, P. E. 1994. "Projector Augmented-Wave Method." *Physical Review B* 50 (24): 17953–79. doi:10.1103/PhysRevB.50.17953.

Braga, D., F. Grepioni, G. I. Lampronti, L. Maini, and A. Turrina. 2011. "Ionic Co-Crystals of Organic Molecules with Metal Halides: A New Prospect in the Solid Formulation of Active Pharmaceutical Ingredients." *Crystal Growth and Design* 11 (12): 5621–27. doi:10.1021/cg201177p.

Bruker. 2014. *Bruker TOPAS 5 User Manual*. Karlsruhe, Germany, Bruker AXS GmbH.

Buikin, P., A. Vologzhanina, R. Novikov, P. Dorovatovskii, and A. Korlyukov. 2023. "Abiraterone Acetate Complexes with Biometals: Synthesis, Characterization in Solid and Solution, and the Nature of Chemical Bonding." *Pharmaceutics* 15 (9): 2180. doi:10.3390/pharmaceutics15092180.

Coelho, A. A. 2003. "Indexing of Powder Diffraction Patterns by Iterative Use of Singular Value Decomposition." *Journal of Applied Crystallography* 36 (1): 86–95. doi:10.1107/S0021889802019878.

Dhondale, M. R., P. Thakor, A. G. Nambiar, M. Singh, A. K. Agrawal, N. R. Shastri, and D. Kumar. 2023. "Co-Crystallization Approach to Enhance the Stability of Moisture-Sensitive Drugs." *Pharmaceutics* 15 (1): 189. doi:10.3390/pharmaceutics15010189.

Goloveshkin, A. S., A. A. Korlyukov, and A. V. Vologzhanina. 2021. "Novel Polymorph of Favipiravir — An Antiviral Medication." *Pharmaceutics* 13 (2): 139. doi:10.3390/pharmaceutics13020139.

Guerain, M., P. Derollez, L. Roca-Paixão, C. Dejoie, N. T. Correia, and F. Affouard. 2020. "Structure Determination of a New Cocrystal of Carbamazepine and Dl-tartaric Acid by Synchrotron Powder X-ray Diffraction." *Acta Crystallographica Section C: Structural Chemistry* 76 (3): 225–30. doi:10.1107/S2053229620000868.

Hilfiker, R., F. Blatter, & M. V. Raumer. 2006. Relevance of Solid-state Properties for Pharmaceutical Products in R. Hilfiker (Ed.), *Polymorphism* (pp. 1–19). Wiley. doi:10.1002/3527607889.ch1

Hotter, A., A. Pichler, V. Adamer, & U. Griesser. 2013. "Novel Polymorph of Rilpivirine Hydrochloride." World Intellectual Property Organization Patent WO2013153161A2. https://patents.google.com/patent/WO2013153161A2/en?oq=WO2013153161A2.

Kaduk, J. A., K. Zhong, and T. N. Blanton. 2015. "Crystal Structure of Rilpivirine, $C_{22}H_{18}N_6$." *Powder Diffraction* 30 (2): 170–74. doi:10.1017/S0885715615000196.

Kaduk, J. A., S. Gates-Rector, and T. N. Blanton. 2023a. "Crystal Structure of Besifloxacin Hydrochloride, $C_{19}H_{22}ClFN_3O_3Cl$." *Powder Diffraction* 38 (1): 43–52. doi:10.1017/S0885715622000586.

Kaduk, J. A., S. Gates-Rector, and T. N. Blanton. 2023b. "Crystal Structure of Butenafine Hydrochloride, $C_{23}H_{28}NCl$." *Powder Diffraction* 38 (1): 30–6. doi:10.1017/S0885715622000562.

Kommavarapu, P., A. Maruthapillai, K. Palanisamy, and M. Sunkara. 2015. "Preparation and Characterization of Rilpivirine Solid Dispersions with the Application of Enhanced Solubility and Dissolution Rate." *Beni-Suef University Journal of Basic and Applied Sciences* 4 (1): 71–9. doi:10.1016/j.bjbas.2015.02.010.

Korlyukov, A. A., P. V. Dorovatovskii, and A. V. Vologzhanina. 2022. "N-(4-Methyl-3-((4-(pyridin-3-yl)pyrimidin-2-yl)amino) phenyl)-4-((4-methylpiperazin-1-yl)methyl)benzamide." *Molbank* 2022 (4): M1461. doi:10.3390/M1461.

Korlyukov, A. A., P. A. Buikin, P. V. Dorovatovskii, and A. V. Vologzhanina. 2023. "Synthesis, NoSpherA2 Refinement, and Noncovalent Bonding of Abiraterone Bromide Monohydrate." *Structural Chemistry* 34 (5): 1927–34. doi:10.1007/s11224-023-02210-3.

Kresse, G., and J. Furthmüller. 1996a. "Efficiency of Ab-initio Total Energy Calculations for Metals and Semiconductors using a Plane-Wave Basis Set." *Computational Materials Science* 6 (1): 15–50. doi:10.1016/0927-0256(96)00008-0.

Kresse, G., and J. Furthmüller. 1996b. "Efficient Iterative Schemes for Ab initio Total-Energy Calculations Using a Plane-Wave Basis Set." *Physical Review B - Condensed Matter and Materials Physics* 54 (16): 11169–86. doi:10.1103/PhysRevB.54.11169.

Kresse, G., and J. Hafner. 1993. "Ab Initio Molecular Dynamics for Liquid Metals." *Physical Review B* 47 (1): 558–61. doi:10.1103/PhysRevB.47.558.

Kresse, G., and J. Hafner. 1994. "Ab Initio Molecular-Dynamics Simulation of the Liquid-Metal–Amorphous-Semiconductor Transition in Germanium." *Physical Review B* 49 (20): 14251–69. doi:10.1103/PhysRevB.49.14251.

Kresse, G., and J. Hafner. 2000. "First-Principles Study of the Adsorption of Atomic H on Ni (111), (100) and (110)." *Surface Science* 459 (3): 287–302. doi:10.1016/S0039-6028(00)00457-X.

Kresse, G., and D. Joubert. 1999. "From Ultrasoft Pseudopotentials to the Projector Augmented-Wave Method." *Physical Review B* 59 (3): 1758–75. doi:10.1103/PhysRevB.59.1758.

Momma, K., and F. Izumi. 2011. "VESTA 3 for Three-Dimensional Visualization of Crystal, Volumetric and Morphology Data." *Journal of Applied Crystallography* 44 (6): 1272–76. doi:10.1107/S0021889811038970.

O'Boyle, N. M., M. Banck, C. A. James, C. Morley, T. Vandermeersch, and G. R. Hutchison. 2011. "Open Babel: An Open Chemical Toolbox." *Journal of Cheminformatics* 3 (1): 33. doi:10.1186/1758-2946-3-33.

Paulekuhn, G. S., J. B. Dressman, and C. Saal. 2007. "Trends in Active Pharmaceutical Ingredient Salt Selection based on Analysis of the Orange Book Database." *Journal of Medicinal Chemistry* 50 (26): 6665–72. doi:10.1021/jm701032y.

Perdew, J. P., S. Kurth, A. Zupan, and P. Blaha. 1999. "Accurate Density Functional with Correct Formal Properties: A Step Beyond the Generalized Gradient Approximation." *Physical Review Letters* 82 (12): 2544–47. doi:10.1103/PhysRevLett.82.2544.

Putcharoen, O., S. J. Kerr, and K. Ruxrungtham. 2013. "An Update on Clinical Utility of Rilpivirine in the Management of HIV Infection in Treatment-Naive Patients." *HIV/AIDS – Research and Palliative Care* 5 (September): 231–41. doi:10.2147/HIV.S25712.

https://doi.org/10.1017/S0885715624000228 Published online by Cambridge University Press

Rendell, J., A. Mittelman, M. Erlich, and M. Ratkaj. 2012. "Solid State Forms of Rilpivirine Base, and Rilipivirine salts." World Intellectual Property Organization Patent WO2012125993A1. https://patents.google.com/patent/WO2012125993A1/en?oq=WO2012125993A1+

Rietveld, H. M. 1967. "Line Profiles of Neutron Powder-Diffraction Peaks for Structure Refinement." *Acta Crystallographica* 22 (1): 151–52. doi:10.1107/S0365110X67000234.

Sandoz, A. Z. 2013. "Novel Crystalline Form of Rilpivirine Hydrochloride." European Patent EP2628732A1. https://patents.google.com/patent/EP2628732A1/de?oq=EP2628732A1

Stokbroekx, S. C. M. 2010. "Crystalline Form of 4-[[4-[[4-(2-cyanoethenyl)-2,6-dimethylphenyl]-amino]-2-pyrimidinyl]amino]benzonitrile." US Patent US20100189796A1. https://patents.google.com/patent/US20100189796A1/en?oq=US2010189796

Surov, A. O., K. V. Drozd, A. G. Ramazanova, A. V. Churakov, A. V. Vologzhanina, E. S. Kulikova, and G. L. Perlovich. 2023. "Polymorphism of Carbamazepine Pharmaceutical Cocrystal: Structural Analysis and Solubility Performance." *Pharmaceutics* 15 (6): 1747. doi:10.3390/pharmaceutics15061747.

Svetogorov, R. D. 2018. *Dionis – Diffraction Open Integration Software*. Moscow, National Research Center Kurchatov Institute.

Svetogorov, R. D., P. V. Dorovatovskii, and V. A. Lazarenko. 2020. "Belok/XSA Diffraction Beamline for Studying Crystalline Samples at Kurchatov Synchrotron Radiation Source." *Crystal Research and Technology* 55 (5): 1900184. doi:10.1002/crat.201900184.

Wermuth, C. G., and P. H. Stahl. 2001. *Pharmaceutical Salts, Properties, Selection, and Use. A Handbook*. Zürich, Helvetica Chimica Acta/Wiley-VCH.

https://doi.org/10.1017/S0885715624000228 Published online by Cambridge University Press